Stability of Gravity-Stabilized Drag-Free Satellites

ALAN W. FLEMING* AND DANIEL B. DEBRA†
Stanford University, Stanford, Calif.

In a drag-free satellite, the relative position sensor null point and the thrustor lines of action will not be coincident with the vehicle mass center. Thus, attitude motion is sensed by the translation control system. The resulting coupling between the attitude and translational motions can cause attitude instabilities in a gravity stabilized drag-free satellite. In some cases the phase shift which degrades the stability is introduced by the orbital dynamics in a unique interaction of the feedback with the passive attitude control and orbital mechanics. Stability relationships derived from small perturbation linear analysis are discussed and compared with results from a nonlinear analog simulation with derived rate translational control.

A. Introduction

A DRAG-FREE satellite contains an unsupported proof mass which is shielded by the satellite from external nongravitational forces. Since only gravitational forces act on the proof mass, it follows a purely gravitational orbit. A control system in the satellite senses motion of the satellite relative to the proof mass and activates thrusters, forcing the satellite to follow the proof mass without touching it (Fig. 1). Therefore, the satellite also follows a purely gravitational orbit, free from the effects of external surface forces.

A drag-free orbit is useful in satellite geodesy, for navigation satellites where accurate ephemeris prediction is needed, and for determining the drag on a satellite by measuring the equal and opposite compensating thrust, as Lange[1] has proposed.

A drag-free satellite may use any type of attitude control and, in principle, there need not be any orientation-translation coupling. In practice coupling exists due to the combination of two effects. First, thrusters not acting through the satellite mass center produce torques which disturb the attitude motion, and secondly, if the proof-mass sensor null is not at the satellite mass center, its output contains contributions from orientation as well as translation.

For a gravity stabilized satellite, two kinds of torques may thus be induced by attitude perturbations. The first is a direct torque which is in phase (or 180° out of phase) with the attitude motion. Torques of this nature have only minor effect on stability since the magnitude of the torque is assumed small with respect to gravity restoring torques. The second kind of torque is an indirect one that contains an extra integration due to the natural coupling of the system dynamics. This torque is 90° (or 270°) out of phase with the attitude motion and can easily add energy to the motion faster than it is being removed by the system damping.

This paper discusses the effect of coupling on the stability of gravity-stabilized, drag-free satellites.

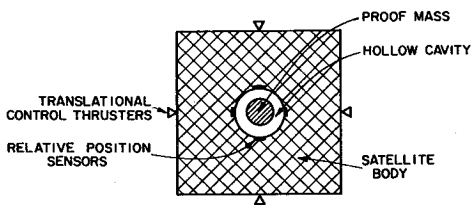

Fig. 1 Planar schematic of a drag-free satellite.

B. Equations of Motion

1. General Form of the Equations

For any drag-free satellite, four relationships are needed to define the vehicle motion. Making the necessary assumptions to obtain a set of linear equations, taking the Laplace Transform and ignoring disturbances, these relationships are

Translation Dynamics

$$A\bar{\delta r} = \sum_{j=1}^{3} \bar{F}^j \tag{1}$$

Orientation Dynamics

$$B\bar{\theta} = \sum_{j=1}^{3} \bar{L}^j \times \bar{F}^j \tag{2}$$

Sensor Equation

$$\bar{e}^j = -[(\bar{\delta r} + \bar{\theta} \times \bar{\epsilon}) \cdot \hat{c}_j]\hat{c}_j \tag{3}$$

Control Law

$$\bar{F}^j = K\bar{e}^j \tag{4}$$

where (see Fig. 2), $\bar{\delta r}$ is the position vector of the satellite mass center with respect to its disturbance free equilibrium position of $r = -\bar{\epsilon}$; $\bar{\theta}$ is the small angle attitude vector of the vehicle with respect to a local tangent reference frame (torque-free equilibrium orientation); A, B, and K are linear operators to

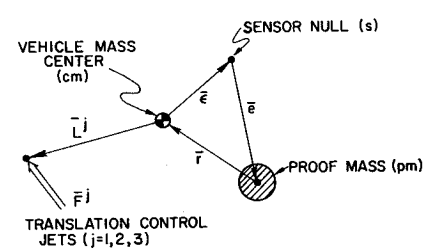

Fig. 2 Schematic of drag-free satellite geometry.

Presented as Paper 70-995 at the AIAA Guidance Control and Flight Mechanics Conference, Santa Barbara, Calif., August 17–19, 1970; submitted August 24, 1970; revision received April 19, 1971. The authors gratefully acknowledge the support of this research under subcontract APL/JHU 271881 through the Applied Physics Laboratory of the Johns Hopkins University under prime contract N-00017-62-C-0604.

Index categories: Spacecraft Attitude Dynamics and Control; Spacecraft Navigation, Guidance, and Flight-Path Control Systems.

* Research Engineer, Department of Aeronautics and Astronautics. Member AIAA.

† Associate Professor, Department of Aeronautics and Astronautics. Associate Fellow AIAA.

be discussed later; $\bar{F}^j$ ($j = 1,2,3$) is the jth control force assuming both positive and negative thrusters for a given direction pass through a common point; $\bar{L}^j$ ($j = 1,2,3$) is the moment arm of the jth control force about the satellite mass center; $\bar{e}^j$ is the output of the jth position sensor; $\bar{\epsilon}$ is the location of the position sensor null with respect to the vehicle mass center; and $\hat{c}_j$ ($j = 1,2,3$) defines a right-handed set of orthogonal unit vectors aligned with the directions of the translation control forces.

The characteristic equation of this system may be obtained by direct substitution of Eqs. (3) and (4) into Eq. (1), solving for $\bar{\delta}r$ and substituting this into Eq. (2) to get a single vector equation in $\bar{\theta}$:

$$\left\{B + K\left[\sum_{j=1}^{3}(\bar{L}^j \times \hat{c}_j)(\hat{c}_j \cdot)\right] \cdot [K(A + KU)^{-1} - U](\bar{\epsilon}\times)\right\}\bar{\theta} = 0 \quad (5)$$

where U is the unity operator. The determinant of the coefficient operator set equal to zero (for a nontrivial solution) is the characteristic equation.

2. Reference Frame Definitions

Referring to Fig. 3, the "orbital frame," (o), is defined by a unit vector $\hat{o}_1$ along the orbital radius pointing away from the Earth, a unit vector $\hat{o}_2$ in the in-track direction of orbital motion, and a third unit vector $\hat{o}_3$ normal to the orbit plane, completing the right-handed set. The second frame (b), defined by the three unit vectors $\hat{b}_1$, $\hat{b}_2$, and $\hat{b}_3$, is fixed in the satellite and aligned with the principal axes of inertia for the vehicle mass center. The orientation of (b) with respect to (o) is specified by a set of three Euler angles as shown in the figure. All quantities, such as forces and moment arms, are fixed in the body (see Fig. 2) except the translation, $\bar{\delta}r$, which is most naturally expressed in the orbital reference frame. The controller reference frame $\hat{c}_1$, $\hat{c}_2$, $\hat{c}_3$ will be taken to coincide with the body frame $\hat{b}_1$, $\hat{b}_2$, $\hat{b}_3$.

3. Coefficient Matrices

The orbital translation perturbation equations due to Hill are well known (e.g., Lange[1]). The in-plane motion is coupled and A, written in the o frame, becomes

$$A = \begin{bmatrix} ms^2 - 3m\omega_0^2 & -2m\omega_0 s & 0 \\ 2m\omega_0 s & ms^2 & 0 \\ 0 & 0 & ms^2 + m\omega_0^2 \end{bmatrix} \quad (6)$$

where ω_0 is the oribital angular velocity and m is vehicle mass.

If the attitude behavior is lightly damped ($\zeta \ll 1$), nonlinearities in the damping mechanism do not have a great effect on the fine structure of the resulting motion and linear damping may be assumed with adequate accuracy for this study. Assuming a gravity-stabilized system with yaw stability augmented with a constant speed pitch wheel, B in Eq. (2) becomes (Pisacane[2] and Crespo da Silva[3])

$$B = \begin{bmatrix} I_1 s^2 + D_1 s + (I_3 - I_2)\omega_0^2 + h\omega_0 & [(-I_1 - I_2 + I_3)\omega_0 + h]s & 0 \\ -[(-I_1 - I_2 + I_3)\omega_0 + h]s & I_2 s^2 + D_2 s + 4(I_3 - I_1)\omega_0^2 + h\omega_0 & 0 \\ 0 & 0 & I_3 s^2 + D_3 s + 3(I_2 - I_1)\omega_0^2 \end{bmatrix} \quad (7)$$

where I_1, I_2, and I_3 are principal inertias of the vehicle for the mass center, h is the magnitude of the angular momentum of a roll-yaw coupling momentum wheel with its spin axis along $\hat{b}_3$, and D_1, D_2, and D_3 are attitude damping coefficients.

4. Characteristic Equation

With the assumption that translation response is very much faster than orbital frequency, terms containing ω_0^2 in $[K(A + KU)^{-1} - U]$ may be dropped. In addition, it is assumed that the controllers are (on the average) linear functions of $\bar{e}$ and $\dot{\bar{e}}$, $K = (k_v s + k_p)U$. Then the characteristic equation of the entire six-degree-of-freedom system may be written out using Eqs. (6) and (7) in Eq. (5)

$$\det\left\{B - \frac{(k_v s + k_p)(ms^2)}{(ms^2 + k_v s + k_p)} \cdot \begin{bmatrix} -(L_3{}^2\epsilon_3 + L_2{}^3\epsilon_2) & L_2{}^3\epsilon_1 & L_3{}^2\epsilon_1 \\ L_1{}^3\epsilon_2 & -(L_3{}^1\epsilon_3 + L_1{}^3\epsilon_1) & L_3{}^1\epsilon_2 \\ L_1{}^2\epsilon_3 & L_2{}^1\epsilon_3 & -(L_2{}^1\epsilon_2 + L_1{}^2\epsilon_1) \end{bmatrix} + \frac{(k_v s + k_p)^2(2m\omega_0 s)}{(ms^2 + k_v s + k_p)^2} \cdot \begin{bmatrix} 0 & -L_3{}^2\epsilon_3 & +L_3{}^2\epsilon_2 \\ L_3{}^1\epsilon_3 & 0 & -L_3{}^1\epsilon_1 \\ -L_2{}^1\epsilon_3 & +L_1{}^2\epsilon_3 & (L_2{}^1\epsilon_1 - L_1{}^2\epsilon_2) \end{bmatrix}\right\} \quad (8)$$

where the subscripts on $\bar{L}^j$ and $\bar{\epsilon}$ denote measure numbers of these vectors in the $\hat{b}_1,\hat{b}_2,\hat{b}_3$ frame. If it is further assumed that $m|\bar{L}^j||\bar{\epsilon}| \ll I_1$, application of the generalized algorithm of Gauss to Eq. (8) yields a characteristic equation which is the product of two factors

$$\left[(I_3 s^2 + D_3 s + I_3\omega_3^2) + \frac{(k_v s + k_p)^2(2m\omega_0 s)(L_2{}^1\epsilon_1 - L_1{}^2\epsilon_2)}{(ms^2 + k_v s + k_p)^2}\right] \times \left[(I_1 s^2 + D_1 s + I_1\omega_1^2)(I_2 s^2 + D_2 s + I_2\omega_2^2) + (Hs)^2 + \frac{ms^2(k_v s + k_p)}{(ms^2 + k_v s + k_p)}(L_1{}^3\epsilon_2 - L_2{}^3\epsilon_1)Hs\right] = 0 \quad (9)$$

where

$$\omega_1^2 \triangleq [(I_3 - I_2)\omega_0^2 + h\omega_0]/I_1, \quad \omega_2^2 \triangleq [4(I_3 - I_1)\omega_0^2 + h\omega_0]/I_2$$

$$\omega_3^2 \triangleq [3(I_2 - I_1)/I_3]\omega_0^2, \quad H \triangleq (-I_1 - I_2 + I_3)\omega_0 + h$$

The first factor of Eq. (9) represents motion in the plane of the orbit. The stability of this motion was discussed in detail by Fleming et al.,[4] and will not be discussed further here.

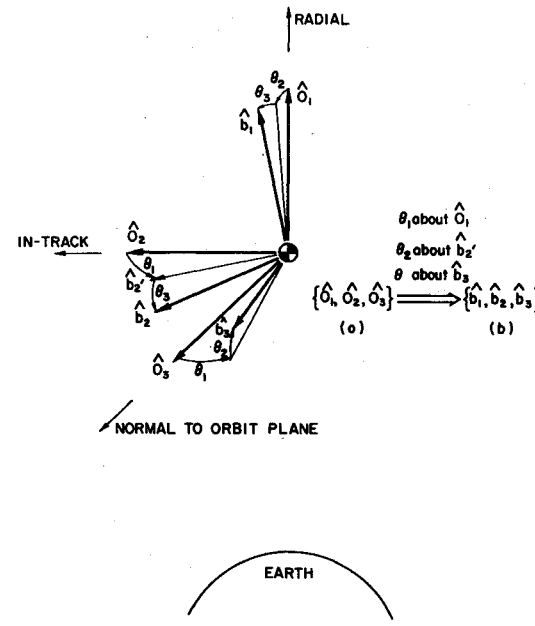

Fig. 3 Definition of body and orbital reference frames.

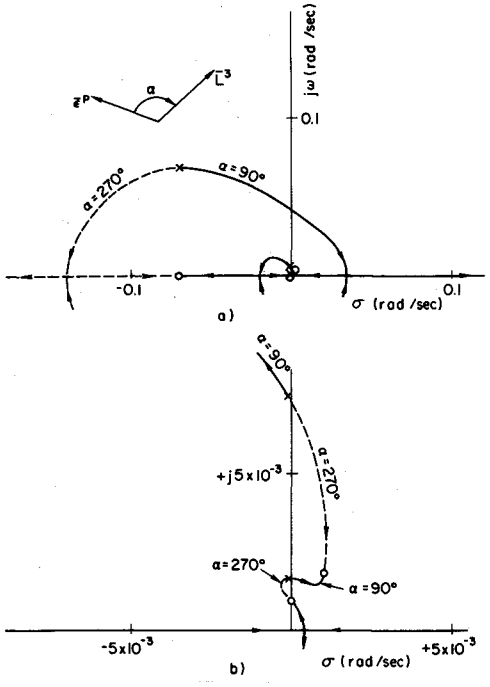

Fig. 4 Root locus for out-of-plane motion as a function of $|\bar{L}^3||\bar{\epsilon}^p| \sin\alpha$ for $\alpha = 90°$ and $\alpha = 270°$.

The second factor represents the out-of-plane motion, which decouples from the in-plane motion due to the assumptions $m|\bar{L}^i||\bar{\epsilon}| \ll I_1$. In Eq. (9), it should be noted that the term containing the control coupling factor $(L_1{}^3\epsilon_2 - L_2{}^3\epsilon_1)$ also contains the factor H, expressing the natural dynamic coupling between roll and yaw. This provides the integration path necessary to obtain a 90° phase shift in torque. (The direct in-phase torque dropped out of Eq. (8) with the assumption that $m|\bar{L}||\bar{\epsilon}| \ll I_1$.)

The quantity $L_1{}^3\epsilon_2 - L_2{}^3\epsilon_1$ may also be written $(\bar{L}^3 \times \bar{\epsilon}) \cdot \hat{b}_3 = |\bar{L}^3||\bar{\epsilon}^p| \sin\alpha$ where α is the angle of $\bar{L}^3$ with respect to the projection of $\bar{\epsilon}, \bar{\epsilon}^p$, on the plane normal to $\hat{b}_3$ (nominally the orbit plane). This notation will be used subsequently to emphasize the importance of the geometrical relationship between $\bar{L}^3$ and $\bar{\epsilon}$.

C. Instability Results

An approximate set of analytical relationships between the system and the vectors $\bar{L}^i$ and $\bar{\epsilon}$ for system instability may be obtained from the characteristic Eq. (9) by, for example, constructing the Routhian array. This will yield the criteria for instability (note the negative value on the first inequality)‡

$$|\bar{L}^3||\bar{\epsilon}^p| \sin\alpha < -\frac{I_1I_2}{Hm(\omega_1{}^2 + \omega_2{}^2 + H^2/I_1I_2)} \times \left[\frac{D_1}{I_1}\left(\omega_1{}^2 + \frac{H^2}{I_1I_2}\right) + \frac{D_2}{I_2}\left(\omega_2{}^2 + \frac{H^2}{I_1I_2}\right)\right]$$

and (10)

$$|\bar{L}^3||\bar{\epsilon}^p| \sin\alpha > +\frac{I_1I_2}{Hm}\left[\frac{D_1}{I_1}\frac{1}{\omega_1{}^2}\left(\omega_2{}^2 + \frac{H^2}{I_1I_2}\right) + \frac{D_2}{I_2}\frac{1}{\omega_2{}^2}\left(\omega_1{}^2 + \frac{H^2}{I_1I_2}\right)\right.$$

The natural roots of the gravity stabilized attitude motion separate into a high-frequency pair with frequency ω_{HF} and damping ζ_{HF} and a low-frequency pair, with ω_{LF} and ζ_{LH}. If $D_1/(I_1\omega_1)$ and $D_2/(I_2\omega_2) \ll 1$, then

$$\omega_{LF} \doteq \omega_1\omega_2[\omega_1{}^2 + \omega_2{}^2 + H^2/I_1I_2]^{-1/2}$$

$$\omega_{HF} \doteq [\omega_1{}^2 + \omega_2{}^2 + H^2/I_1I_2]^{1/2}$$

$$\zeta_{LF} \doteq \frac{\omega_{LF}}{2(\omega_{HF}{}^2 - \omega_{LF}{}^2)}\left\{\frac{D_1}{I_1}\frac{1}{\omega_1{}^2}\left(\omega_2{}^2 + \frac{H^2}{I_1I_2}\right) + \frac{D_2}{I_2}\frac{1}{\omega_2{}^2}\left(\omega_1{}^2 + \frac{H^2}{I_1I_2}\right)\right\}$$

and

$$\zeta_{HF} \doteq \frac{1}{2\omega_{HF}(\omega_{HF}{}^2 - \omega_{LF}{}^2)}\left\{\frac{D_1}{I_1}\left(\omega_1{}^2 + \frac{H^2}{I_1I_2}\right) + \frac{D_2}{I_2}\left(\omega_2{}^2 + \frac{H^2}{I_1I_2}\right)\right\}$$

Inequalities (10) may be further simplified by expressing them in terms of these natural roots of the gravity-stabilized attitude motion rather than the coefficients of the differential equations. Thus

$$|\bar{L}^3||\bar{\epsilon}^p| \sin\alpha < -(2I_1I_2/Hm)[\zeta_{HF}(\omega_{HF}{}^2 - \omega_{LF}{}^2)/\omega_{HF}] \quad (11)$$

and

$$|\bar{L}^3||\bar{\epsilon}^p| \sin\alpha > +(2I_1I_2/Hm)[\zeta_{LF}(\omega_{HF}{}^2 - \omega_{LF}{}^2)/\omega_{LF}] \quad (12)$$

To check the validity of these approximate relationships, the characteristic roots of the roll/yaw portion of the full system equations, Eqs. (1–4), were obtained as a function of $|\bar{L}^3||\bar{\epsilon}^p|$ for various values of α. Figure 4 is a root locus plot for $\alpha = 90°$ and $\alpha = 270°$ with the following typical gravity stabilized system parameters: $m = 86.1$ kg; $I_1 = 21.75$ kg·m²; $I_2 = 560$ kg·m²; $h = 0.571$ N·m·sec; $\omega_0 = 1.02 \times 10^{-3}$ rad/sec; $D_1/I_1 = 2.59 \times 10^{-5}$ rad/sec; $D_2/I_2 = 1.12 \times 10^{-5}$ rad/sec; $\epsilon_1 = \epsilon_2 = 0.02$ rr; $k_p = 0.86$ N/m; $k_v = 12.1$ N·sec/m.

Since the translational control system for motion normal to the orbit plane is much faster than the roll/yaw attitude mo-

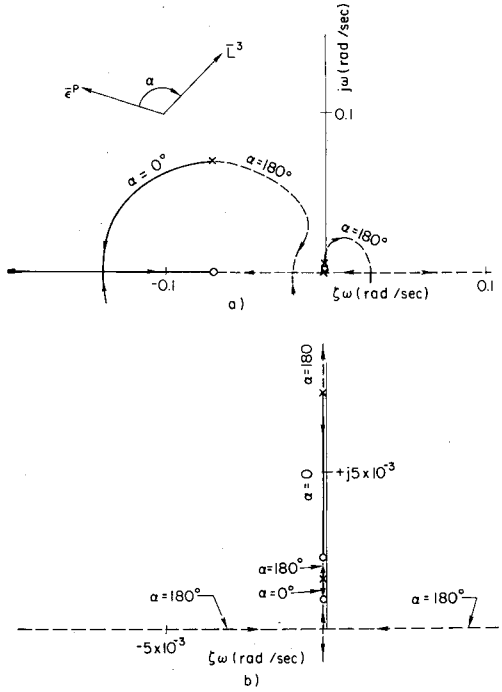

Fig. 5 Root locus for out-of-plane motion as a function of $|\bar{L}^3||\bar{\epsilon}^p| \sin\alpha$ for $\alpha = 0°$ and $\alpha = 180°$.

‡ It is shown in Ref. 4 that the corresponding instability result for the in-plane motion is $(L_1{}^2\epsilon_2 - L_2{}^1\epsilon_1) > D_3/2m\omega_0$.

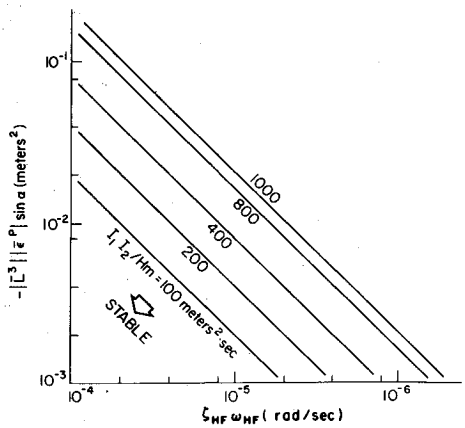

Fig. 6 Roll/yaw instability as a function of system parameters and high-frequency damping.

tion, two views of the loci are necessary. One, Fig. 4a, a macroscopic view, shows translational control response, and the other, Fig. 4b, a microscopic view near the origin, shows attitude response. The instabilities predicted by inequalities (11) and (12) are crossover points of the loci departing from the low frequency poles of the attitude motion.

The predicted high-frequency crossover value ($\alpha = 270°$) from inequality (11) is $-|\bar{L}^3||\bar{\epsilon}^p| = -0.00751$ m^2. This agrees very well with the actual value obtained from the root solutions, -0.00749. The predicted low-frequency crossover ($\alpha = 90°$) from inequality (12) is $|\bar{L}^3||\bar{\epsilon}^p| = +0.0365$ m^2 compared with the actual value of $+0.0637$ m^2. This poor agreement for the low-frequency prediction is due to the fact that for this case $m|\bar{L}^3||\bar{\epsilon}^p| = 5.5$ kg·m^2, and this term cannot be neglected compared with I_1, as was assumed in deriving inequality (12). In terms of the loci, the assumption removes the zero from the right half plane near the low frequency root, allowing the crossover to occur for lower values of $|\bar{L}^3||\bar{\epsilon}^p|$. This inaccuracy in predicting the low-frequency crossover is relatively unimportant since the high-frequency crossover is the one which governs the maximum value of $|\bar{L}^3||\bar{\epsilon}^p|$, for which the system is stable.

Figure 5 is a root locus for the same system but with $\alpha = 0°$ and 180°. These roots reflect the direct (or in-phase) coupling dropped from the analysis in deriving inequalities (11) and (12). For values of $|\bar{L}^3||\bar{\epsilon}^p| < 0.2$ m^2 these loci show that primarily the frequency (not the damping) of the attitude motion is affected. There is a high-frequency crossover in Fig. 5 for $|\bar{L}^3||\bar{\epsilon}^p| \doteq 0.34$ m^2, but this again is out of the valid region for the assumption $m|\bar{L}^3||\bar{\epsilon}^p| \ll I_1$. On comparing Figs. 4 and 5, it should be noted that the 0°/180° departure paths are not orthogonal to the 90°/270° paths since the zeros of the loci are different for the two cases.

For the purpose of specifying a design constraint among the system parameters and $|\bar{L}^3||\bar{\epsilon}^p|$, the high-frequency crossover ($\alpha = 270°$) represented by inequality (11) is shown graphically in Fig. 6.

D. Analog Verification of the Results

For an analog computer simulation of the coupled attitude-translation system, the dynamical equations, Eqs. (1) and (2), and sensor equation,§ Eq. (3), were used directly. A set of runs was made first with strictly linear control to check out the system simulation. The results agreed with the digital results represented by the root loci of Figs. 4 and 5, and the approximate analytical criterion, inequality (11).

§ A capacitive sensor used in a laboratory breadboard exhibits an additional cubic term, but it is negligible for this coupling study. (However, it cannot be neglected in acquisition and transient response studies.)

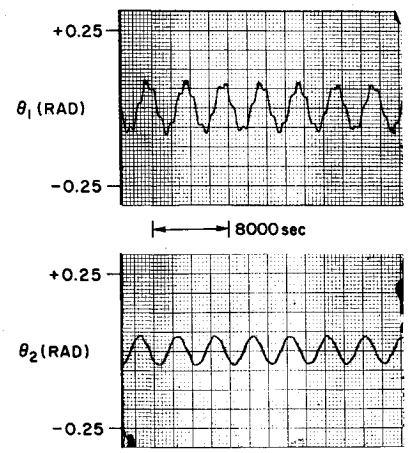

Fig. 7 Yaw and roll vs time for no translational coupling.

Next, to study behavior with a nonlinear controller, a derived rate modulator[5] was assumed to operate each thrustor. This modulator switch with hysteresis is activated by a signal, a^i, which is the difference between the error signal, e^i, and a lagged feedback signal, f^i, from the thrustor:

$$a^i = e^i - kf^i, \quad \tau\dot{f}^i + f^i = F^i \tag{13}$$

The damping is inherent in the lagged feedback. F^i is full on or off but its average value is approximately linear in e^i when averaged over times comparable to the gravity-gradient oscillation period.

From this part of the simulation, it was found that certain characteristics of the nonlinear controller, such as deadband and controller average gain at the deadband threshold, have a major influence on the behavior for various values of α. In particular, the α for which the system is most sensitive can range from about 270° to 180°. However, the magnitude of $|\bar{L}^3||\bar{\epsilon}^p|$ at the high-frequency crossover remains unchanged.

To illustrate this behavior, representative samples of analog output are shown in Figs. 7–11. For these runs, an attempt was made to minimize the influence of deadband by making it as small as possible compared with $\bar{\theta} \times \bar{\epsilon}$. The actual values used were $|\bar{\epsilon}^p| = 0.113$ m, deadband = 0.25 mm, and controller gain at threshold = 0.5 N/m.

Figure 7 shows nominal θ_1 (roll) and θ_2 (yaw) without any translational coupling. Figure 8 is with $\alpha = 270°$ and $|\bar{L}^3||\bar{\epsilon}^p| = 0.00780$ m^2 (slightly beyond the predicted high-frequency crossover). The high frequency is slightly divergent and the low frequency is near nominal. Figure 9 is for $\alpha = 90°$, and $|\bar{L}^3||\bar{\epsilon}^p| = 0.0955$ m^2 (50% over the linear low-frequency crossover of the root locus). The high frequency is

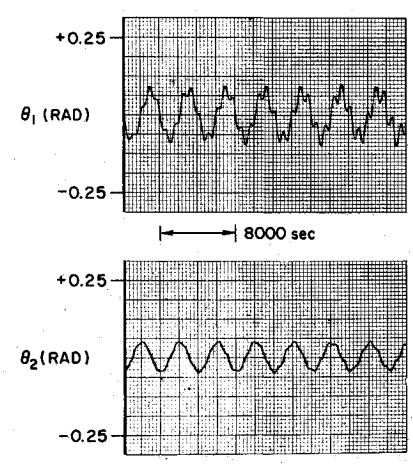

Fig. 8 Yaw and roll vs time for $|\bar{L}^3||\bar{\epsilon}^p| = 0.00780$ m^2 and $\alpha = 270°$ with a derived rate controller.

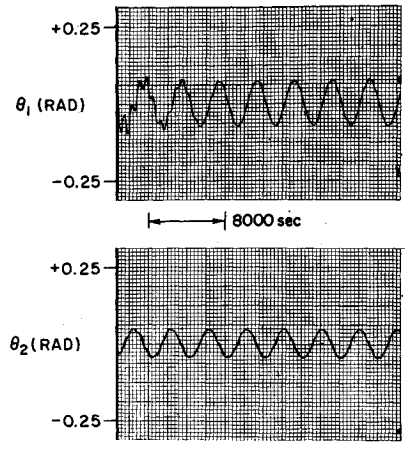

Fig. 9 Yaw and roll vs time for $|\bar{L}^3||\bar{\epsilon}^p| = 0.0955$ m² and $\alpha = 90°$ with a derived rate controller.

very stable and the low frequency is near divergence. Figure 10 is for $\alpha = 0°$, and $|\bar{L}^3|\,|\bar{\epsilon}^p| = 0.0955$ m² (which is the same as for $\alpha = 90°$ in Fig. 9). Both high and low frequencies have about nominal damping and a slight decrease in frequency. Figure 11 is for $\alpha = 180°$ and for $|\bar{L}^3|\,\bar{\epsilon}^p| = 0.0350$. Both frequencies are higher than nominal and the high frequency is almost divergent. This indicates a high-frequency crossover for $\alpha = 180°$ at values of $|\bar{L}^3|\,|\bar{\epsilon}^p|$ less than predicted by the root loci of the linear case. Apparently the nonlinear characteristics of the derived rate controller have an effect equivalent to a change in the pole locations of the translation control dynamics. "On the average," these poles are shifted so they affect the departure angle of the root locus from the high-frequency poles of the attitude motion for $\alpha = 180°$. As a result, this branch of the locus crosses the $j\omega$ axis for smaller values of $|\bar{L}^3|\,|\bar{\epsilon}^p|$ than in the linear case.

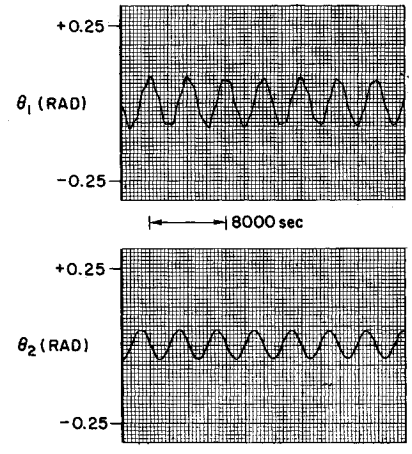

Fig. 10 Yaw and roll vs time for $|\bar{L}^3||\bar{\epsilon}^p| = 0.0955$ m² and $\alpha = 0°$ with a derived rate controller.

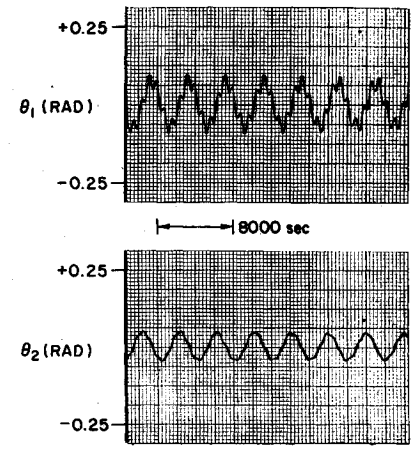

Fig. 11 Yaw and roll vs time for $|\bar{L}^3||\bar{\epsilon}^p| = 0.0350$ m² and $\alpha = 180°$ with a derived rate controller.

In summarizing the nonlinear analog results, it may be said that inequality (11) can be used to predict the minimum magnitude of $|\bar{L}^3|\,|\bar{\epsilon}^p|$ for high-frequency crossover, but the values of α for which this crossover occurs depend on controller characteristics.

E. Conclusion

A criterion [inequality (11)] has been obtained which accurately defines a stability boundary for attitude-translational coupled motion, out of the plane of the orbit, for a gravity-stabilized drag-free satellite. A similar criterion, for motion in the plane of the orbit, has been obtained previously by Fleming et al.[4] These criteria specify allowable translational control sensor null offsets and translational thrustor moment arms as a function of vehicle physical parameters. They may be used for systems with nonlinear translational controllers to specify allowable magnitudes, but the angular relationship between the null offset and thrustor moment arms for which the stability is most sensitive is a strong function of the nonlinear characteristics of the controller.

References

[1] Lange, B. O., "The Drag-Free Satellite," *AIAA Journal*, Vol. 2, No. 9, Sept. 1964, pp. 1590–1606.

[2] Pisacane, V. L., "Three-Axis Stabilization of a Dumbbell Satellite by Small Constant Speed Rotors," APL Rept. TG-855, Oct. 1966, Applied Physics Lab., Johns Hopkins Univ.

[3] Crespo da Silva, M. R. M., "Attitude Stability and Motions of a Gravity-Stabilized-Gyrostat-Satellite in a Circular Orbit," Scientific Rept. 32, Dec. 1968, Stanford Electronics Labs., Stanford Univ.

[4] Fleming, A. W., DeBra, D. B., and Crespo da Silva, M. R. M., "Attitude-Translation Coupling in Drag-Free Satellites," Paper 8.2, *3rd IFAC Symposium on Automatic Control in Space*, Toulouse, France, March 1970.